Published online 27 February 2018

Nucleic Acids Research, 2018, Vol. 46, No. 6 ***3119–3129***
doi: 10.1093/nar/gky154

Noncanonical substrate preference of lambda exonuclease for 5′-nonphosphate-ended dsDNA and a mismatch-induced acceleration effect on the enzymatic reaction

Tongbo Wu[1], Yufei Yang[1,2], Wei Chen[1], Jiayu Wang[1], Ziyu Yang[1], Shenlin Wang[1,2], Xianjin Xiao[3], Mengyuan Li[1] and Meiping Zhao[1,*]

[1]Beijing National Laboratory for Molecular Sciences, MOE Key Laboratory of Bioorganic Chemistry and Molecular Engineering, College of Chemistry and Molecular Engineering, Peking University, Beijing 100871, China, [2]Beijing NMR Center, Peking University, Beijing 100871, China and [3]Family Planning Research Institute/Center of Reproductive Medicine, Tongji Medical College, Huazhong University of Science and Technology, Wuhan 430030, China

Received November 05, 2016; Revised February 16, 2018; Editorial Decision February 16, 2018; Accepted February 19, 2018

ABSTRACT

Lambda exonuclease (λ exo) plays an important role in the resection of DNA ends for DNA repair. Currently, it is also a widely used enzymatic tool in genetic engineering, DNA-binding protein mapping, nanopore sequencing and biosensing. Herein, we disclose two noncanonical properties of this enzyme and suggest a previously undescribed hydrophobic interaction model between λ exo and DNA substrates. We demonstrate that the length of the free portion of the substrate strand in the dsDNA plays an essential role in the initiation of digestion reactions by λ exo. A dsDNA with a 5′ non-phosphorylated, two-nucleotide-protruding end can be digested by λ exo with very high efficiency. Moreover, we show that when a conjugated structure is covalently attached to an internal base of the dsDNA, the presence of a single mismatched base pair at the 5′ side of the modified base may significantly accelerate the process of digestion by λ exo. A detailed comparison study revealed additional π–π stacking interactions between the attached label and the amino acid residues of the enzyme. These new findings not only broaden our knowledge of the enzyme but will also be very useful for research on DNA repair and *in vitro* processing of nucleic acids.

INTRODUCTION

Lambda exonuclease (λ exo) is a 5′→3′ exonuclease that processively digests one strand of a duplex DNA molecule to generate a 3′-single stranded-overhang (1,2). It is involved in the recombination of DNA in bacteriophage lambda (3,4) As a typical member of the PD-(D/E)XK nuclease superfamily (5,6), this enzyme has been extensively studied to understand the mechanism of its high processivity (7–10), its sequence-dependence (11–13) and other factors that may affect the recombination efficiency (14–16). Because of its robust properties and low cost, λ exo is widely used in multiple biotechnology applications, such as genetic engineering using homologous recombination (17,18), the ChIP-exo method for DNA-binding protein mapping (19), nanopore sequencing (20) and biosensors (21–24).

The crystal structure of λ exo reveals a symmetrical toroid homotrimer (25). In the complex with DNA, λ exo unwinds two bases at the 5′ end of the substrate strand to pull it into the reaction center (26). λ exo hydrolyses double-stranded DNA (dsDNA) 130 times faster than single-stranded DNA (ssDNA) (1). A DNA duplex with a 5′ phosphorylated blunt or recessed end is the appropriate substrate for λ exo, while the digestion rate of a dsDNA with a 5′ hydroxyl end or a 5′ phosphorylated overhang is significantly slower (15). The 5′-PO_4 in the substrate was thought to play an essential role in the 'electrostatic ratchet' model; it is much more efficient to initiate the digestion reaction with a 5′-PO_4 than a 5′-OH (26,27). Herein, we demonstrate the results of our recent work on the interactions between λ exo and miscellaneous nucleic acid molecules. First, we show that a DNA duplex with a 5′ non-phosphorylated, two-nucleotide (2-nt) protruding end can be digested by λ exo with very high efficiency, which strongly suggests that the 5′ phosphorylated end is dispensable for λ exo to initiate DNA digestion. Second, we found that in a DNA duplex containing an internal base that has been covalently modified with a conjugated

*To whom correspondence should be addressed. Tel: +86 10 62758153; Fax: +86 10 62751708; Email: mpzhao@pku.edu.cn

structure (e.g. FAM, ROX) via a 1,6-hexanediamine linker, the presence of a single mismatched base pair at the 5′ side of the modified base may significantly accelerate the process of digestion of the labeled strand by λ exo. Possible mechanisms for these unexpected properties were investigated in detail.

MATERIALS AND METHODS

Materials

Lambda exonuclease (λ exo, WT-1) and ThermoPol Reaction Buffer (20 mM Tris–HCl, 10 mM KCl, 10 mM $(NH_4)_2SO_4$, 2 mM $MgSO_4$ and 0.1% Triton X-100, pH 8.8 @ 25°C) were purchased from New England Biolabs (NEB, MA, USA). Wild type (λ exo WT-2) and λ exo variants (λ exo R28A, Y160A, W170A and F172A) were expressed according to the method developed by Zhang *et al.* (26). DNA strands were synthesized and purified by HPLC (Sangon Biotech Co., Shanghai, China). The sequences of all the nucleic acid probes and complementary strands that have been studied in this work are summarized in Supplementary Table S1. The plasmid vector with the gene of λ exo was purchased from Genewiz Biotech Co. (Suzhou, China). The 50-bp DNA ladder, 6× DNA loading buffer, pre-stained protein marker and 2× protein loading buffer were purchased from Tiangen Biotech Co. (Beijing, China). Precast-Glgel 12% SDS-PAGE kit was purchased from Sangon Biotech Co. DNase free deionized water from Tiangen Biotech Co. was used in all the experiments.

Measurement of the digestion rates of λ exo on different nucleic acid duplexes

To a 200 μl PCR tube, 39 μl of water, 5 μl of 10 × ThermolPol Reaction Buffer, 2 μl of probe (10 pmol) and 1 μl of the complementary strand (5 pmol) were added and mixed well. The solution was heated to 85°C and then gradually cooled down to 37°C. Then, 3 μl of λ exo (NEB) was added, and the detection was performed at 37°C on a Rotor-Gene Q 5plex HRM Instrument (QIAGEN, Hilden, Germany). The amount of λ exo as trimer was 0.53 pmol (2.5 U, final concentration 10.6 nM) for Figures 1A and 3, Supplementary Figure S2, S3, S4 and S6A, 0.36 pmol (1.7 U, final concentration 7.2 nM) for Figure 2, Supplementary Figure S5 and S6B, and 0.18 pmol (0.83 U, final concentration 3.6 nM) for Figure 5, Supplementary Figure S7 and S8B. Fluorescence intensity was measured once per cycle (5 s per cycle). The excitation and emission wavelengths were set at 470 and 510 nm, respectively, for the probes labeled with FAM and 585 and 610 nm, respectively, for the probes labeled with ROX. The rate of fluorescence increase was determined by the slope of the linear portion of the time curve. All experiments were repeated at least three times.

Measurement of the K_m and k_{cat} of λ exo for different DNA duplexes

To a 200 μl PCR tube, 41 μl of water, 5 μl of 10× ThermolPol Reaction Buffer, 1 μl of the probe (0.25, 0.5, 0.75, 1, 1.5, 2.25, 3 pmol) and the same amount of complementary strands were added and mixed well. The solution was heated to 85°C and then gradually cooled down to 37°C. Then, 1 μl of λ exo (NEB, 0.053 pmol, 0.25 U, final concentration 1.06 nM) was added and the detection was performed at 37°C on a Stratagene Mx3000P instrument (New York, USA) with a gain level of 8. Fluorescence intensity was measured once per cycle (5 s per cycle) until the fluorescence signals reached a plateau. The excitation and emission wavelengths were set at 470 nm and 510 nm, respectively.

Gel electrophoresis analysis

In Figure 1C, agarose gel electrophoresis was carried out using a 2.5% agarose gel at 120 V in a 0.5× TBE buffer (90 mM Tris, 90 mM boric acid, 2 mM EDTA; pH 8.0). The samples were prepared in a 200 μl PCR tube with 38 μl of water, 5 μl of 10× ThermolPol Reaction Buffer, 2 μl of probe (40 pmol) and 2 μl of the complementary strand (40 pmol). The solution was heated to 85°C and then gradually cooled down to 37°C. Then, 3 μl of λ exo (NEB, 1.1 pmol, 5 U, final concentration 22 nM) was added, and the reaction was performed at 37°C. After 0, 40, 80 or 200 min, the reaction was terminated by heating the solution to 85°C to deactivate λ exo. Then, 9 μl of sample solution and 1.8 μl of loading buffer were mixed and added to each well. 6 μl of 50 bp DNA ladder was used as a marker and loaded in the leftmost lane. After separation, the gels containing DNA were stained using the nucleic acid dye GelSafe (excitation wavelength 302 nm, emission wavelength 590 nm, Yuanpinghao Bio, Beijing, China) and visualized at a wavelength of 590 nm using a Tanon 1600 gel imaging system (Tanon, China).

In Supplementary Figure S8A, polyacrylamide gel electrophoresis was carried out using the Precast-Glgel 12% SDS-PAGE kit at 180 V. Equal volumes (10 μl) of sample solution and loading buffer were mixed and added to each well. After separation, the gels were stained using Coomassie brilliant blue (CBB) fast staining solution purchased from Tiangen Biotech Co. and visualized at a wavelength of 590 nm using a Tanon 1600 gel imaging system.

RESULTS

The reactions between λ exo and different dsDNA substrates were monitored by using fluorescently labeled DNA duplexes. As shown in Scheme 1A, dual-labeled ssDNA fluorescent probes (Supplementary Table S1, the names begin with P-) were hybridized to their complementary strands (Supplementary Table S1, the names begin with C-) with or without mismatched bases. The distance between the fluorophore (FAM or ROX) and the quencher (BHQ-1 or BHQ-2) was in the range from 11 bases (∼3.7 nm) to 26 bases (∼8.2 nm); thus, the fluorescence of the intact probe was very weak due to fluorescent energy resonance transfer (FRET) (28). Once the probe strand was digested by λ exo and the nucleotide containing the FAM group was released from the duplex, strong fluorescent signals could be observed. Since all the probes had a labeled 3′ end (Supplementary Table S1) and all the complementary strands had a 5′-OH end, the digestion from the 5′ end of the complementary strands by λ exo was efficiently blocked (22–24), and thus, the obtained DNA duplexes could be used to evaluate the effects of different chemical modifications, introduced

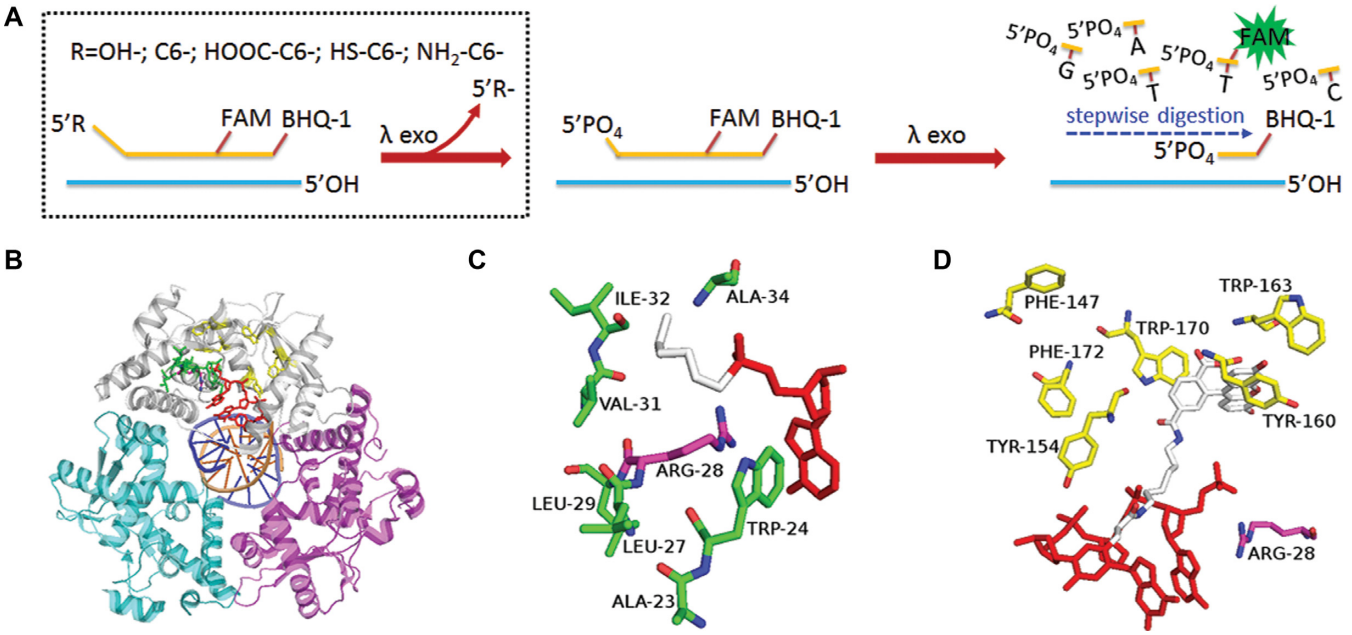

Scheme 1. (**A**) Schematic depiction of the principle of the method used to investigate the reactions between λ exo and different dsDNA substrates. (**B**) The proposed hydrophobic interaction area (green) and π–π stacking interaction area (yellow) marked in the crystal structure of λ exo with 5′-PO_4 DNA duplex (PDB 3SM4). The 5′ end of the DNA strand was indicated in red. (**C**) The proposed hydrophobic interaction between the hydrophobic amino acid residues (green) in λ exo and the C6 spacer modification (grey) at the 5′ end of the DNA strand (red). (**D**) The proposed π–π stacking interaction between the amino acid residues (yellow) in λ exo and the FAM tag (gray) labeled at the third nucleotide from the 5′ end of the DNA strand (red). R28 was shown in purple (with the N atoms in blue) in (B), (C) and (D). The dataset of the protein-DNA complex structure was obtained from PDB 3SM4 and drawn with Pymol. The C6 spacer and FAM were drawn with Pymol.

at the 5′ end of the probe (as shown in the dash frame in Scheme 1A) or at the internal bases, on the digestion rates of the probe strand by λ exo. The concentrations of λ exo used in the fluorescent assays (3.6–10.6 nM for wild-type λ exo and 32–84 nM for λ exo variants) were all lower than that of the dsDNA substrate (100 nM). The digestion rates of the duplexes by λ exo were determined by calculation based on the rate of fluorescence increase of the reaction solution under the tested conditions.

Digestion of dsDNA substrates with 5′-nonphosphate ends by λ exo

DNA duplexes with 5′-OH ends can be digested faster in the presence of a 2-nt overhang structure at the 5′ end. In comparison with the DNA duplexes with 5′-PO_4 ends, 5′-OH-ended dsDNAs have been reported to be poor substrates for λ exo. Thus, λ exo hydrolyses 5′-PO_4 dsDNA more than 300 times faster than 5′-OH dsDNA (1). In our experiments, however, we noted that the digestion of 5′-OH ended DNA duplex by λ exo could proceed when the first two bases near the 5′ end were unpaired with the bases in the opposite strand. As shown in Figure 1, the perfectly matched (PM) duplex of P1-5'OH-6FAM/C1-PM(42) could hardly be digested by λ exo. But the presence of a mismatched base pair in the duplex at the second position from the 5′ end (P1-5'OH-6FAM/C1-2-mis(42) duplex) remarkably enhanced the digestion rate, reaching approximately 3.8% of that for the 5′-PO_4 counterparts (P2-5'PO_4-6FAM/C1-PM(42), Supplementary Figure S2). In contrast, the introduction of single mismatched base pairs at other positions near the 5′ end, such as at the first (C1-1-mis(42)), third (C1-3-mis(42)) and fourth (C1-4-mis(42)) positions, or double mismatched base pairs at the first/third (C1-1,3-mis(42)) or second/fourth (C1-2,4-mis(42)) positions, all slightly inhibited the cleavage reactions by λ exo (see detailed results in Figure 1A and Supplementary Figure S2). According to a previous report, dsDNA with a penultimate mismatch may be regarded as bearing a two-nucleotide (2-nt) overhang structure, with no hydrogen bonding between the terminal matched base pair (29). Thus, the above results suggest that λ exo could bind and digest a dsDNA substrate with a 2-nt overhang at the 5′-OH end. To validate this, we changed the sequence of C1-PM(42) and prepared a number of different overhang-structures at the 5′-OH end. As shown in Figure 1A and B and Supplementary Figure S3, among the tested 5′-OH DNA duplexes with different lengths of overhang (from 2-nt to 5-nt), all the DNA duplexes with a 2-nt overhang structure were quickly digested by λ exo. The cleavage rate was enhanced more than 20-fold in comparison with the 5′-OH PM counterparts (P1-5'OH-6FAM/C1-PM(42)). For the 5′-PO_4 duplexes, the digestion rate of P2-5'PO_4-6FAM/C1-2-mis(42) was generally the same as that of the P2-5'PO_4-6FAM/C1-PM(42) (Supplementary Figure S2).

To further confirm the digestion reaction, we synthesized an unlabeled probe (P1'-5'OH-unlabeled, Supplementary Table S1), which had the same sequence as P1-5'OH-6FAM but without the FAM label. Then, we performed the same hydrolytic reactions on P1-5'OH-6FAM/C1-2-mis(42) and P1'-5'OH-unlabeled/C1-2-mis(42) duplexes. Additionally, the P1'-5'OH-6FAM/C1-PM(42) and P1'-

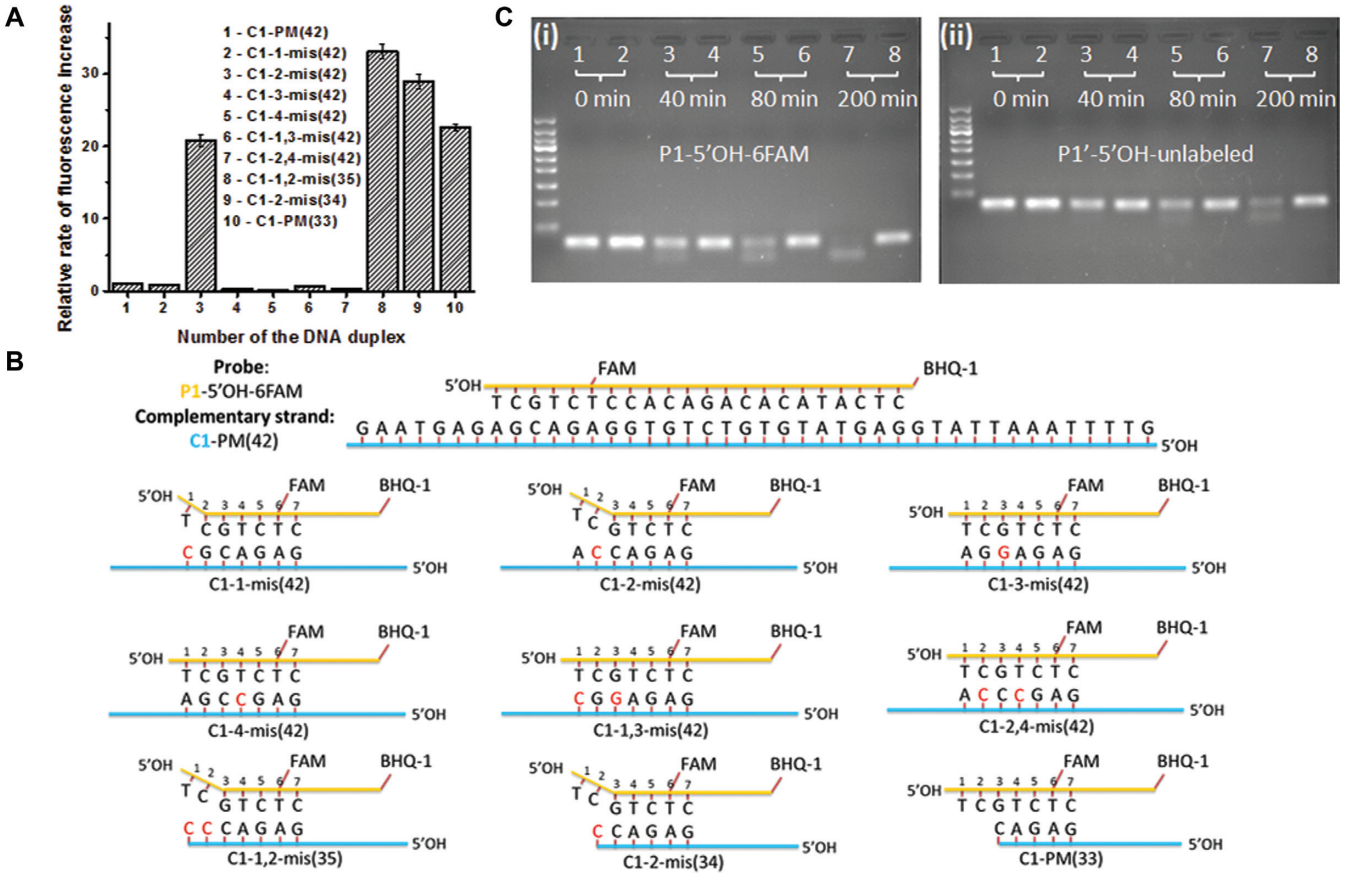

Figure 1. The digestion of different 5′-OH DNA duplexes by λ exo. (**A**) The relative digestion rates of P1-5'OH-6FAM duplexes. The rate of fluorescence increase of P1-5'OH-6FAM/C1-PM(42) is set to 1.0. Error bars represent the standard deviation from experiments performed in triplicate. (**B**) The schematic structures of different P1-5'OH-6FAM duplexes. The complete sequence of the P1-5'OH-6FAM/C1-PM(42) duplex is shown. In the schematic structures, only the first seven base pairs from the 5′ end of the labeled probe are shown to highlight the variation of the sequences near 5′ end in comparison with the P1-5'OH-6FAM/C1-PM(42) duplex. Other parts of all the tested duplexes are identical. The mismatched bases are indicated in red in the tested mismatched DNA duplexes. (**C**) Agarose gel electrophoresis results for the duplexes after reacting with λ exo for different period of time. (i) P1-5'OH-6FAM/C1-2-mis(42) (lane 1, 3, 5 and 7), P1-5'OH-6FAM/C1-PM(42) (lanes 2, 4, 6 and 8), (ii) P1'-5'OH-unlabeled/C1-2-mis(42) (lane 1, 3, 5 and 7) and P1'-5'OH-unlabeled/C1-PM(42) (lanes 2, 4, 6 and 8).

5'OH-unlabeled/C1-PM(42) duplexes were also tested for comparison. The reaction products were collected and analysed with agarose gel electrophoresis. Both P1-5'OH-6FAM/C1-2-mis(42) and P1'-5'OH-unlabeled/C1-2-mis(42) duplexes were gradually digested after 40 min, as can be clearly seen from the faded bands and newly formed bands in Figure 1C (lanes 1, 3, 5, 7). In contrast, for the corresponding PM-duplexes, the bands remained almost unchanged, indicating very slow digestion rates (Figure 1C, lanes 2, 4, 6, 8). The results were consistent with those obtained in the fluorescence analysis (Figure 1A).

To test the generality of this new property of λ exo, we synthesized another probe with a different sequence from P1-5'OH-6FAM and with the fluorophore labeled at a different position, P3-5'OH-15FAM (Supplementary Table S1). Similar enhancement effects of the 2-nt overhang structure on the cleavage rate were observed for DNA duplexes formed by P3-5'OH-15FAM and different complementary strands (Supplementary Figure S4), although the enhancement ratio was only approximately 10-fold, which is lower than those observed in Figure 1A. These results confirmed that with a 2-nt overhang structure, 5′-OH DNA duplexes could be digested faster by λ exo.

The digestion of DNA duplexes by **λ** *exo can be efficiently initiated by multiple terminal structures at the 5′ end.* To investigate whether the 5′-PO_4 end can be displaced with other groups, we changed the group at the 5′ end of probe P3-5'OH-15FAM to C6 spacer, carboxyl-C6, sulfhydryl-C6, and amino-C6 (as shown in the dash frame in Scheme 1A. Supplementary Figure S1A shows the structures of these modifications), corresponding to probes P5-5'C6-15FAM, P6-5'COOH-15FAM, P7-5'HS-15FAM, and P8-5'NH_2-15FAM, respectively (Supplementary Table S1). In comparison with the P3-5'OH-15FAM/C2-PM(42)-duplex, most of the PM-duplexes of these new probes were digested much faster by λ exo (Figure 2 and Supplementary Figure S5), and the 2-mis-duplexes were digested even faster than their PM counterparts (Table 1). Furthermore, as shown in Table 1, the 2-mis-duplexes consisting of P5-5'C6-15FAM, P6-5'COOH-15FAM and P7-5'HS-15FAM were digested almost as fast as the P9-5'PO_4-15FAM/C2-PM(42) duplex, which strongly suggests that in

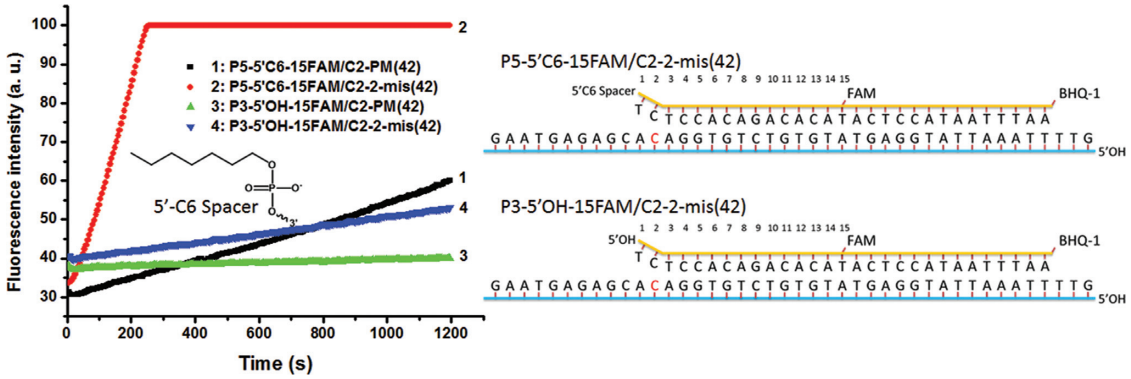

Figure 2. Time courses of the digestion reactions of P3-5'OH-15FAM and P5-5'C6-15FAM duplexes by λ exo. The schematic structures of P3-5'OH-15FAM/C2-2-mis(42), P3-5'OH-15FAM/C2-2-mis(42) and 5'C6 spacer are shown. The mismatched bases are indicated in red.

Table 1. Relative rates of fluorescence increase of different PM- and 2-mis-duplexes digested by λ exo (WT-1)

Probe	PM	2-mis	Raito of 2-mis to PM
P3-5'OH-15FAM	0.0079 ± 0.0003	0.067 ± 0.002	8.5 ± 0.4
P5-5'C6-15FAM	0.087 ± 0.004	1.12 ± 0.03	12.9 ± 0.7
P6-5'COOH-15FAM	0.123 ± 0.004	0.94 ± 0.02	7.6 ± 0.3
P7-5'HS-15FAM	0.135 ± 0.004	0.97 ± 0.03	7.2 ± 0.3
P8-5'NH_2-15FAM	0.021 ± 0.001	0.45 ± 0.02	22 ± 2
P9-5'PO_4-15FAM	1.00 ± 0.05	1.13 ± 0.05	1.13 ± 0.07

The rate of fluorescence increase of P9-5'PO_4-15FAM/C2-PM(42) was set to 1.0. The relative rates of fluorescence increase of the duplexes of other probes were calculated based on that of P9-5'PO_4-15FAM/C2-PM(42). The complementary strands used were C2-PM(42) and C2-2-mis(42), respectively.

a DNA duplex with a 2-nt overhang at the 5′ end, these 5′-nonphosphate ends could also efficiently initiate DNA digestion by λ exo.

The 5′-OH ended DNA duplex with 3-nt overhang is digested faster than that with 2-nt overhang. From above experimental results, a 2-nt overhang structure seems to be essential for λ exo to degrade the substrate without a 5′-PO_4 end. Being curious about how λ exo 'counts' the number of the nucleotides at 5′ end, we tested a probe with an abasic site (AP) at the first position from the 5′ end (P11-5'OH-dSpacer-15FAM). The length of the AP modification is approximately equal to that of a nucleotide (Supplementary Figure S1A). Interestingly, the 5'OH-dSpacer duplex with a 3-nt overhang structure (P11-5'OH-dSpacer-15FAM/C2-PM(30)) was digested faster than other counterparts with 0-nt, 1-nt, 2-nt, 4-nt or 5-nt overhang structures (Figure 3A), implying that for 5'OH duplexes, a 3-nt overhang was actually the optimum length of the 5′ free strand for λ exo to initiate the digestion. Similar results were also obtained for other P11-5'OH-dSpacer-15FAM duplexes with 3-nt overhangs (Supplementary Figure S6A). For the P3-5'OH-15FAM duplexes, as shown in Figure 3B, the digestion rate of P3-5'OH-15FAM/C2-PM(29) with a 3-nt overhang was the highest, which was ∼12% of that of the blunt 5′-PO_4 substrate (P9-5'PO_4-15FAM/C2-PM(42)). In P3-5'OH-15FAM and P11-5'OH-dSpacer-15FAM, the FAM label was located far away from the 5′ end (at the fifteenth nucleotide from the 5′ end) and may not affect the interaction of λ exo with the 5′ end. On the other hand, the FAM label in P1-5'OH-6FAM was located near the 5′ end (at the sixth nucleotide from the 5′ end) and thus may affect the digestion of duplexes with a 3-nt overhang structure by λ exo. Therefore, the results of P3-5'OH-15FAM and P11-5'OH-dSpacer-15FAM duplexes were more typical for the duplexes with a 5′ hydroxyl end.

We then re-examined the duplexes of P5-5'C6-15FAM for comparison. As shown in Supplementary Figure S6B, the duplex with a 2-nt overhang (P5-5'C6-15FAM/C2-PM(30)) was digested faster than other duplexes with a 0-nt, 1-nt, 3-nt or 4-nt overhang structure. This implies that the digestion mechanism of the duplexes with a 5′ hydroxyl may be different from that of the duplexes with 5′ hydrophobic modifications.

Digestion of dsDNA substrates with 5′-nonphosphate ends by a λ exo R28A variant. The R28 residue in λ exo was believed to directly electrostatically interact with the 5′-PO_4 of the DNA duplex; thus, the R28A variant had much lower activity on the 5′-PO_4 substrates (10,26). This was confirmed in our work by the measurement of the digestion rates of P9-5'PO_4-15FAM/C2-PM(42) by normal λ exo (WT-1 from NEB) and the R28A variant that we expressed (Figure 4). We then employed another probe, P10-5'FAM, which had a 5′-FAM end and shared the same sequence with P9-5'PO_4-15FAM near the 5′ end (Supplementary Table S1). Since the 5′-FAM also had a hydrophobic linker (Supplementary Figure S1A) as the other tested 5′-nonphosphate ends (Scheme 1A), once the first phosphodiester bond at the 5′ end of P10-5'FAM was cleaved by the enzyme, the FAM tag would be released from the probe and emit a strong fluorescence signal. The results in Figure 4 compares the rates of fluorescence increase of the PM and the 2-mis duplexes of P9-5'PO_4-15FAM, P5-5'C6-15FAM and P10-5'FAM. Since the activity of the R28A variant on

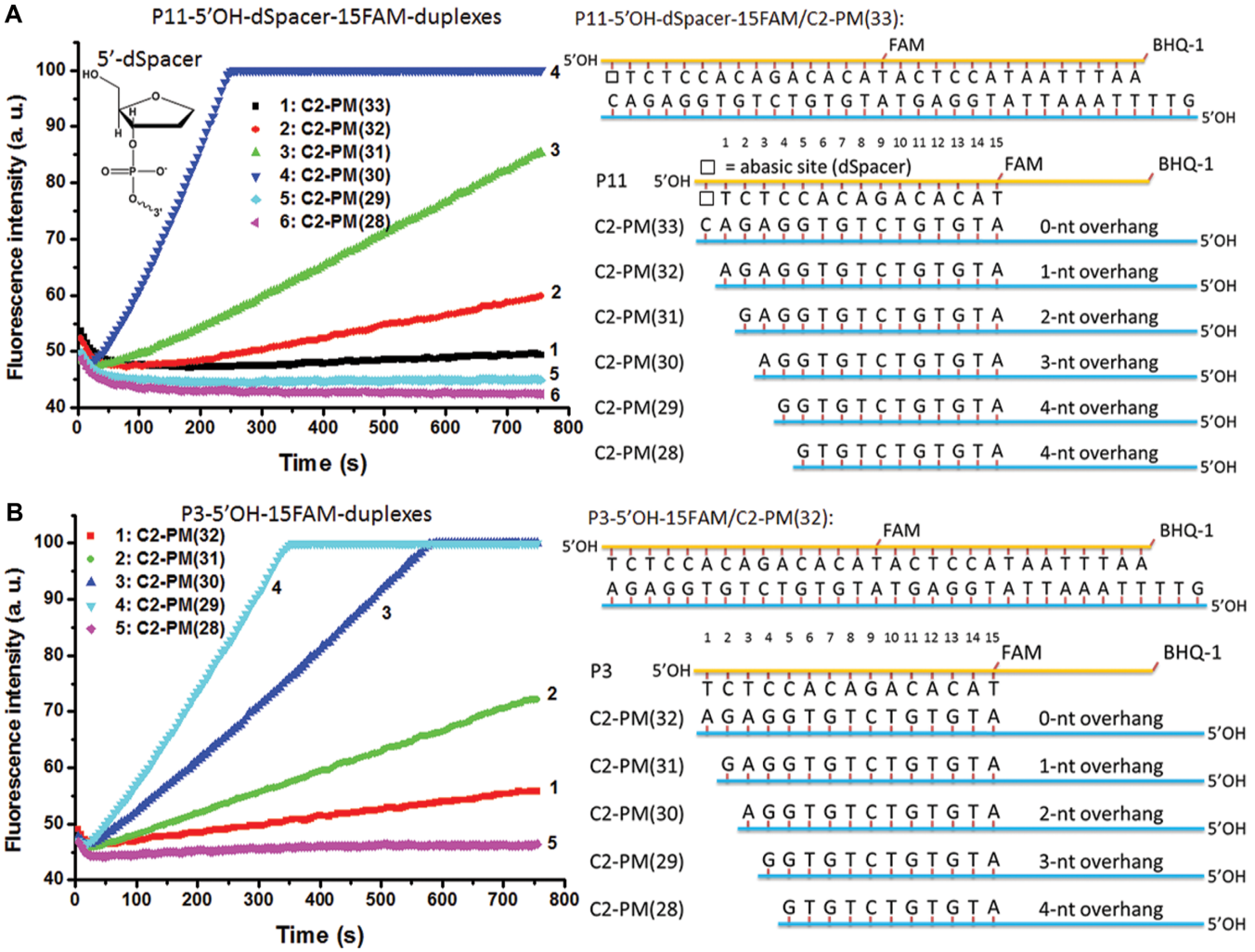

Figure 3. (**A**) Time courses of the digestion reactions of P11-5'OH-dSpacer-15FAM-duplexes by λ exo. The schematic structure of P11-5'OH-dSpacer-15FAM duplexes and 5'-dSpacer are shown. (**B**) Time courses of the digestion reactions of P3-5'OH-15FAM duplexes by λ exo. The schematic structures of P3-5'OH-15FAM-duplexes are shown.

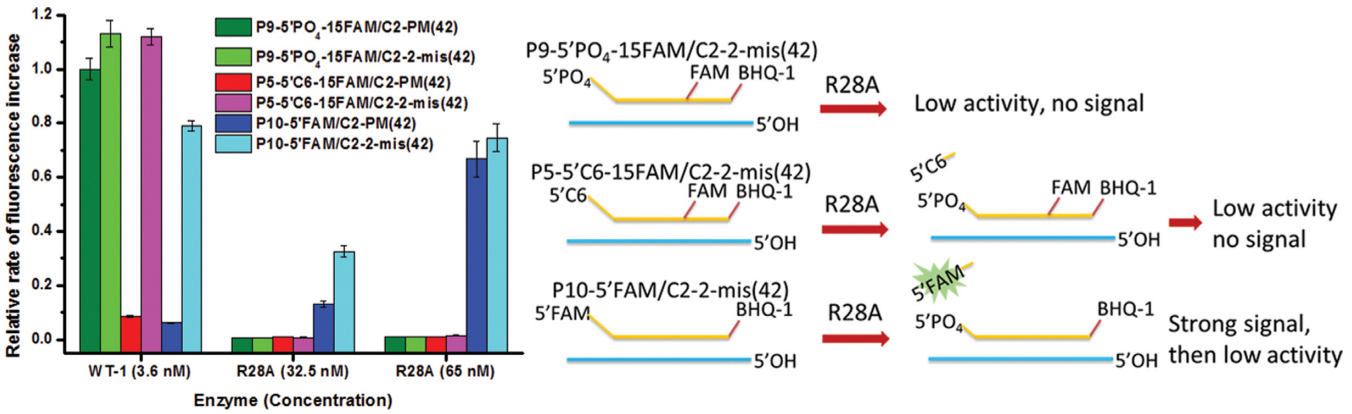

Figure 4. The relative rates of fluorescence increase of the P9-5'PO_4-15FAM/C2-PM(42), P9-5'PO_4-15FAM/C2-2-mis(42), P5-5'C6-15FAM/C2-PM(42), P5-5'C6-15FAM/C2-2-mis(42), P10-5'FAM/C2-PM(42) and P10-5'FAM/C2-2-mis(42) by λ exo WT-1 and R28A variant at different enzyme concentrations. The rate of fluorescence increase of P9-5'PO_4-15FAM/C2-PM(42) digested by 3.6 nM of λ exo WT-1 was set to 1.0. The reaction processes of the three duplexes are schematically depicted.

the 5′-PO_4 substrate was much lower than that of WT-1, we increased the enzyme concentration of R28A to compare its digestion capability on different duplexes. In the presence of more enzyme, we expected to facilitate the initial binding of the R28A variant to the dsDNA substrates (16). Thus, the degradation of the probe strand would lead to an increase in fluorescence, which is used to evaluate the influence of the 2-nt overhang structure. Figure 4 shows that with the increase of the concentration of R28A, the digestion rates of P10-5'FAM/C2-PM(42) duplexes also significantly increased, indicating that in the absence of electrostatic forces, the hydrophobic interactions between the R28A variant and the hydrophobic label at the 5′ end could even enable the digestion of PM duplexes. Moreover, the digestion rate of the P10-5'FAM/C2-2-mis(42) duplexes was further enhanced due to the 2-nt overhang structure, which further supports the hydrophobic interaction mechanism we proposed. With regard to the P5-5'C6-15FAM duplexes, as explained in Figure 4, although the first phosphodiester bond at the 5′ end could be excised by R28A, the resulting 5′-PO_4 substrate could not be further digested even at the higher enzyme concentration due to the lack of electrostatic forces from the positively charged amino acid residues in the active site of the R28A variant. Thus, no fluorescence signals were observed.

Influences of internal chemical modifications on the digestion rates of 5′-PO_4 ended dsDNA by λ exo

Influences of FAM tag on the digestion rates of DNA duplexes containing mismatched base pairs at different positions. We further investigated the influences of modifications on internal bases with neighboring mismatched base pairs in the dsDNA substrates on the digestion rate of λ exo. Previous work revealed that the PM DNA duplex with a 5′-PO_4 end was the most preferred substrate of λ exo and the presence of mismatched base pairs in the duplex tended to slow down the digestion rates (16). In our experiments with the internally labeled dsDNA substrates containing a single mismatch, we found that the relative rate of increase of fluorescence varied significantly with the change of the position of the mismatched bases. As shown in Figure 5A, the mismatched base pairs neighboring the FAM tag (at Position 3 from the 5′ end) had larger influence on the digestion rates of P13-5'PO_4-3FAM/C3-duplexes than those at other positions. Compared to the PM duplex, an acceleration effect of the 2-mismatched base pair on the digestion rate of the P13-5'PO_4-3FAM/C3-duplex was observed. To differentiate the contribution of the fluorophore tag from that of the mismatched base pairs to the acceleration effect, we tested another probe P9-5'PO_4-15FAM which had the same sequence as P13-5'PO_4-3FAM near the 5′ end but with the FAM tag moved to the fifteenth nucleotide from the 5′ end (Position 15). As shown in Figure 5B, the results of the P9-5'PO_4-15FAM duplexes with a single mismatched base pair were quite different from those of the P13-5'PO_4-3FAM duplexes. The P9-5'PO_4-15FAM/C3-2-mis duplex was digested only slightly faster than the P9-5'PO_4-15FAM/C3-PM duplex. By contrast, the P9-5'PO_4-15FAM/C3-14-mis duplex exhibited the highest acceleration effect. As the FAM was labeled at Position 15 from the 5′ end in P9-5'PO_4-15FAM, these results imply that the duplex which had a mismatched base pair at the 5′ side of the FAM-labeled nucleotide would be digested faster than the corresponding PM-duplex. To confirm this, we tested two other probes with the FAM labeled at either the tenth (P14-5'PO_4-10FAM) or the fifty-sixth (P15-5'PO_4-56FAM) nucleotide from the 5′ end. The results in Supplementary Figure S7 substantially supported the above assumption as P14-5'PO_4-10FAM/C4-9-mis was digested faster than P14-5'PO_4-10FAM/C4-PM and P15-5'PO_4-56FAM/C5-55-mis was digested faster than P15-5'PO_4-56FAM/C5-PM.

Mismatch-induced acceleration effect with different internal modifications. We prepared six new probes with different kinds of internal labels (the structures are shown in Supplementary Figure S1B) at Position 3 from the 5′ end, including P16-5'PO_4-3digoxin-15FAM, P17-5'PO_4-3BHQ, P18-5'PO_4-3biotin-15FAM, P19-5'PO_4-3NH_2-15FAM, P20-5'PO_4-3ROX-15FAM and P21-5'PO_4-3FAM-15ROX. The relative digestion rates of their 2-mis-duplexes and 14-mis-duplexes in comparison to the corresponding PM-duplexes are compared in Table 2.

Table 2 shows that almost all the 2-mis-duplexes were digested faster than the PM-duplexes (the relative rate of fluorescence increase > 1.0). Since P9-5'PO_4-15FAM had no labels at Position 3, the 2-mis acceleration effect on the digestion of the P9-5'PO_4-15FAM duplex was mainly due to the 2-nt overhang structure at the 5′ end. Therefore, we employed P9-5'PO_4-15FAM as a reference probe to evaluate the contribution of the label itself to the acceleration effect on the digestion rate of the 2-mis-duplexes of the other probes. Using the ratio of the digestion rate of P9-5'PO_4-15FAM/C3-2-mis to that of P9-5'PO_4-15FAM/C3-PM as the control, we evaluated the differences between the 2-mis and PM duplexes of other probes by Student's t-test. As shown in Supplementary Table S2, the t values larger than 4.032 indicated that there is a significant difference between the digestion rates of the 2-mis and PM duplexes ($P<0.01$, $n' = 5$). Thus, the FAM, ROX and BHQ-1 tags at Position 3 all had an appreciable contribution to the total acceleration effect on the digestion rate of 2-mis-duplexes, while the influence of the other tested tags on the 2-mis acceleration effect was insignificant. These results led us to propose that the FAM, ROX and BHQ-1 tags at Position 3 have synergistic effects with their 5′ mismatched base pair. It is likely that in the presence of the 5′ mismatched base pair, the conjugated structures in FAM, ROX and BHQ-1 were able to interact with certain amino acid residues in the active site of λ exo and facilitate the digestion of the DNA strand by the enzyme. In contrast, the interactions between the other three tags (digoxin, amino and biotin) and the enzyme were negligible.

We also measured the enzyme kinetics (K_m and k_{cat} values) of the digestion reactions of the PM-, 2-mis- and 14-mis-duplexes of P13-5'PO_4-3FAM, P9-5'PO_4-15FAM, P16-5'PO_4-3digoxin-15FAM, P17-5'PO_4-3BHQ and P19-5'PO_4-3NH_2-15FAM, respectively. The results in Supplementary Table S3 show that for the mismatched duplexes that had the remarkable acceleration effect with the label at Position 3, the K_m and k_{cat} values increased proportionally in comparison with their corresponding PM-duplexes.

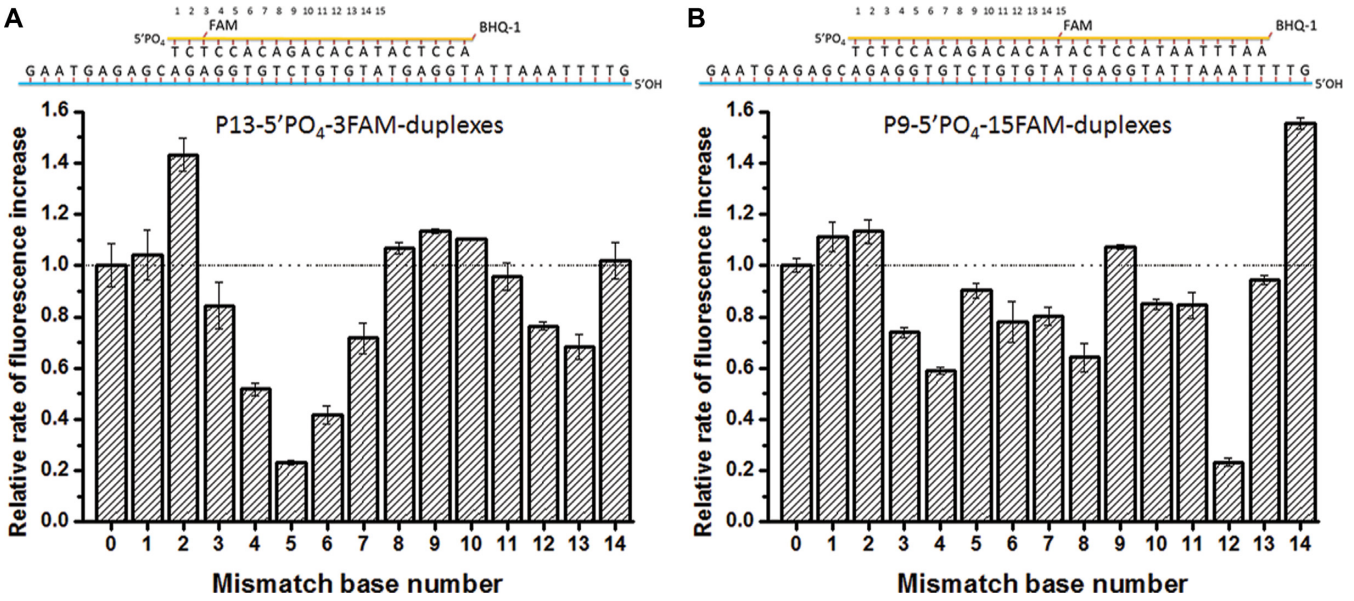

Figure 5. The relative rates of fluorescence increase of the P13-5'PO_4-3FAM (**A**) and P9-5'PO_4-15FAM (**B**) duplexes with single mismatch. The rates of fluorescence increase of P13-5'PO_4-3FAM/C3-PM (A) and P9-5'PO_4-15FAM/C3-PM (B) were set to 1.0 for the two probes, respectively. The schematic structures of P13-5'PO_4-3FAM/C3-PM and P9-5'PO_4-15FAM/C3-PM duplexes are shown.

Table 2. Relative rates of fluorescence increase of the 5′-PO_4 DNA duplexes with different internal labels at Position 3 and mismatched base pairs at two different positions[a]

Probe	Labels at Position 3		Mismatched duplexes	
	Name	Conjugated structure	2-mis	14-mis
P13	FAM	Yes	1.43 ± 0.06	1.01 ± 0.07
P16	digoxin	No	1.18 ± 0.06	1.50 ± 0.07
P17	BHQ-1	Yes	1.56 ± 0.09	0.926 ± 0.005
P18	Biotin	No	1.00 ± 0.06	1.26 ± 0.10
P19	-NH_2	No	1.14 ± 0.04	1.74 ± 0.03
P20[b]	ROX	Yes	1.39 ± 0.03	0..81 ± 0.02
P20[c]	ROX	Yes	1.55 ± 0.02	0.91 ± 0.05
P21[d]	FAM	Yes	1.51 ± 0.06	0.37 ± 0.01
P21[e]	FAM	Yes	1.43 ± 0.01	0.18 ± 0.02
P9	None	-	1.13 ± 0.05	1.55 ± 0.02

[a]The probes shown in this Table were P9-5'PO_4-15FAM, P13-5'PO_4-3FAM, P16-5'PO4-3digoxin-15FAM, P17-5'PO_4-3BHQ, P18-5'PO_4-3biotin-15FAM, P19-5'PO_4-3NH_2-15FAM, P20-5'PO_4-3ROX-15FAM and P21-5'PO_4-3FAM-15ROX, respectively. The rate of fluorescence increase of the PM duplex was set to 1.0 for each probe.
[b,e]The rate of fluorescence increase was calculated based on the signal from ROX channel.
[c,d]The rate of fluorescence increase was calculated based on the signal from FAM channel.

These features strongly implies that some non-productive binding between λ exo and the dsDNA substrate had been converted to productive binding in the presence of the internal label with neighbouring mismatched base pairs at the 5′ side (30). On the other hand, for the mismatched duplexes that showed no acceleration effect with the label at Position 3, the K_m and k_{cat} values were generally similar to those of their corresponding PM-duplexes.

Verification of the mismatch-induced acceleration effect on the digestion of 5′-PO_4 ended dsDNA substrates containing internal labels by different **λ** *exo variants.* The amino acid residues Phe147, Tyr154, Tyr160, Trp163, Trp170 and Phe172 near the reaction center of λ exo all have a conjugated side chain. Thus, these amino acid residues might interact with the labels possessing a conjugated structure via π–π stacking interactions and affect the reaction rate. To confirm this, we expressed three variants of λ exo (Y160A, W170A and F172A) by mutating the amino acid residues containing a conjugated structure to Ala. The wild type λ exo (WT-2) was also expressed in the same way as a control (Supplementary Figure S8A). As shown in Supplementary Figure S8B, in comparison with the WT-2, all the variants showed decreased activity in hydrolysing the PM substrate (P12-5'PO_4-3FAM/C3-PM). We then used the variants to hydrolyse the 2-mis duplex substrates. Table 3 shows that for the probes labeled with FAM and ROX that had a conjugated structure, we observed more remarkable acceleration effects in the digestion of their 2-mis duplexes by λ exo variants in comparison to WT-2. On the other hand, for the probes labeled with either digoxin, biotin or amino groups

that had no conjugated structures, the performance of the λ exo variants was generally similar to that of WT-2.

DISCUSSION

The digestion of a dsDNA substrate by λ exo is believed to proceed through 'an electrostatic ratchet mechanism' that involves five steps (26): (i) bind to the backbone of the ds-DNA; (ii) unwind two nucleotides at the 5′ end; (iii) attract the phosphate at the 5′ end of the dsDNA to the positively charged pocket and locate the first phosphodiester bond to the active center of the enzyme; (iv) hydrolyse the phosphodiester bond and form a new 5′ phosphorylated end; (v) the 5′-PO_4 end strand moves forward and Step four is repeated until the strand is totally digested. For the duplexes containing a 2-mismatched base pair, the second step is not necessary. Therefore, the non-phosphate groups at the 5′ end mainly affect the third step. According to the results in Table 1, the third step can be driven not only by negatively charged groups such as phosphate, carboxyl and sulfhydryl but also by neutral groups such as a C6 spacer, and positively charged groups such the amino group, implying that other forces may exist between the positively charged pocket of λ exo and the 5′ end structure of the DNA substrate. Based on the reported structure of λ exo (26), there are many hydrophobic amino acid residues distributed in the positively charged pocket (in which Arg28 plays a central role) such as Trp24, Leu27, Leu29, Val31, Ile32 and Ala34. This gave us a hint that the hydrophobic interaction area near the active site of λ exo might be able to interact with the 5′ hydrophobic modifications in a similar way as what occurs between the positively charged pocket and the 5′-PO_4 group. As shown in Scheme 1B and C, the C6 spacer at the 5′ end (gray) may interact with the hydrophobic residues (green) in the active site. For other non-phosphate groups linked to the 5′ end via the C6 spacer, the hydrophobic interactions may also draw them to the reaction center and enable the hydrolysis of the first phosphodiester bond at the 5′ end. Once the first phosphodiester bond at the 5′ end is hydrolysed, the resulting 5′-PO_4 end would continue to drive the subsequent digestion reaction in the regular way.

For the 5′-nonphosphate dsDNA substrates containing a 2-mismatched base pair, the C6 spacer, carboxyl-C6 and sulfhydryl-C6 could almost fully displace the function of phosphate to initiate the digestion reaction (Table 1, the relative ratios are as high as 1.12, 0.94 and 0.97 compared to the rate of P9-5'PO_4-15FAM/C2-PM(42)). The P5-5'C6-15FAM/C2-2-mis(42) duplex with a neutral 5′-C6 end that could only interact with the proposed hydrophobic interaction region was digested even slightly faster than those with negatively charged 5′-COOH-C6 or 5′-HS-C6 ends that could also interact with the positively charged pocket. This suggests that the electrostatic interactions (with -COOH or -HS) did not fully complement with the hydrophobic forces (with -C6). For the P8-5'NH_2-15FAM/C2-2-mis(42) duplex with the positively charged 5′ end, the repulsive force from the positively charged pocket of λ exo would counteract the hydrophobic interactions between the C6 spacer and the hydrophobic area, resulting in a lower digestion rate (the relative rate compared to the rate of P9-5'PO_4-15FAM/C2-PM(42) is only 0.45).

For the 5′-nonphosphate PM duplexes, the digestion rates by λ exo were all much slower than the corresponding 5′-PO_4 PM duplex, suggesting that the phosphate group at the 5′ end plays an important role in the unwinding process of the first two nucleotides. However, according to previous studies (10,26), four apolar residues (Val73, Ala75, Ala77, and Leu78) rather than the phosphate are directly involved in the splitting of the two base pairs at the 5′ end. We inferred that the strong electrostatic interactions between the phosphate and the positively charged site in the pocket may provide significant driving forces to facilitate the unwinding of the nucleotides. Under the reaction conditions (pH 8.8), the phosphate group has two negative charges, while the carboxyl and sulfhydryl groups both have only one negative charge; thus, the digestion rates of P6-5'COOH-15FAM/C2-PM(42) and P7-5'HS-15FAM/C2-PM(42) were only as high as 12.3% and 13.5%, respectively, of that of the P9-5'PO_4-15FAM/C2-PM(42) (Table 1). On the other hand, the PM-duplex containing positively charged modifications (amino-C6) at 5′ end barely supported any digestion reaction.

The results for 5′-OH duplexes shown in Figure 3 were slightly different from those of the dsDNA with 5′ hydrophobic modifications. Since the effective distance of hydrophobic interactions (such as those proposed between the 5′-C6 and the hydrophobic amino acid residues of the enzyme) were usually shorter than that of the electrostatic interactions (between 5′-PO_4 and the positively charged amino acid residues), the hydrophobic interactions might become significant only after the first two base pairs are unwound. For the 5′-OH duplexes, the interactions between the hydroxyl group and the electrostatic interaction area or the hydrophobic interaction area are both very weak. It most likely requires a longer free region at the 5′-OH end for the first scissile phosphate to be correctly positioned at the reaction center. Therefore, with a 3-nt overhang structure at the 5′ end, the binding of the 5′-OH strand to the active site of λ exo is greatly facilitated. This led to the observation of the more efficient digestion of the substrate strand.

The results in Section 1 (Digestion of dsDNA substrates with 5′-nonphosphate ends by λ exo) suggest that with a proper length of the flexible 5′ end strand and hydrophobic modifications at the 5′ end, the 5′-PO_4 end is dispensable to the initiation of DNA digestion by λ exo due to an alternative hydrophobic interaction mechanism. This non-canonical substrate preference of the enzyme was substantially confirmed by experiments involving the R28A variant.

The results in Section 2 (Influences of internal chemical modifications on the digestion rates of 5′-PO4 ended ds-DNA by λ exo) suggest that the presence of a mismatched base pair at the 5′ side of the internal label with a conjugated structure (FAM, ROX and BHQ-1) can significantly accelerate the digestion rate of λ exo. We propose that these labels might be able to interact with certain amino acid residues in the active site of λ exo via π–π stacking interactions, which facilitates the digestion of the DNA strand. As depicted in Scheme 1B and 1D, the FAM tag may interact with Tyr160, Trp163 and Trp170. As the 1,6-hexanediamine linker between the tag and the first nucleotide was flexible,

Table 3. The relative ratio of the reaction rates of 2-mis-duplex to PM-duplex for different probes digested by the obtained WT-2 and different variants of λ exo

Probe	Labels at Position 3		λ exo variants[a]			
	Name	Conjugated structure	WT-2	Y160A	W170A	F172A
P13-5'PO_4-3FAM	FAM	Yes	1.40 ± 0.12	1.79 ± 0.08	3.61 ± 0.56	1.53 ± 0.12
P20-5'PO_4-3ROX-15FAM[b]	ROX	Yes	1.30 ± 0.04	1.63 ± 0.05	2.13 ± 0.39	1.60 ± 0.15
P20-5'PO_4-3ROX-15FAM[c]	ROX	Yes	1.53 ± 0.10	2.27 ± 0.06	2.56 ± 0.46	1.64 ± 0.15
P16-5'PO_4-3digoxin-15FAM	Digoxin	No	1.15 ± 0.03	1.34 ± 0.06	1.01 ± 0.18	1.13 ± 0.09
P18-5'PO_4-3biotin-15FAM	Biotin	No	1.04 ± 0.06	1.35 ± 0.09	1.03 ± 0.14	0.94 ± 0.06
P19-5'PO_4-3NH_2-15FAM	-NH_2	No	1.09 ± 0.09	1.20 ± 0.09	1.15 ± 0.08	1.11 ± 0.14
P9-5'PO_4-15FAM	none	-	1.03 ± 0.07	1.09 ± 0.04	1.00 ± 0.10	1.06 ± 0.09

[a]The rate of fluorescence increase of the PM duplex was set to 1.0 for each probe. The concentrations of λ exo (as trimer) used for the reactions were 3.6 nM for WT-2, 7.2 nM for Y160A, 19.8 nM for W170A and 84 nM for F172A, respectively. Under these enzyme concentrations, the digestion rates of the tested PM duplexes were at a similar level so that the enhancement effects of the 2-mis duplexes could be compared with each other.
[b]The rate of fluorescence increase was calculated based on the signal from ROX channel.
[c]The rate of fluorescence increase was calculated based on the signal from FAM channel.

FAM might also interact with Phe147, Tyr154 and Phe172 in the opposite direction.

The kinetic measurement results shown in Supplementary Table S2 suggest that a part of the non-productive binding between λ exo and dsDNA substrates becomes a productive binding when the internally labeled base has an adjacent mismatched base pair at the 5′ side. We infer from the data that the wound PM-duplex forms a natural non-productive binding complex with λ exo, while the complex of λ exo and dsDNA with the first two base pairs at the 5′ end dissociated forms a productive binding complex (Supplementary Scheme S2A). The possible interactions between λ exo and PM or 2-mis DNA duplexes with the internally labeled base located at two different positions are proposed in Supplementary Scheme S2B. For the 2-mis DNA duplex, the label containing a conjugated structure could move more flexibly; thus, its π–π stacking interactions with the amino acid residues of λ exo that contains a conjugated structure were stronger than those of the PM substrate. This additional interaction might be helpful for the formation of more productive binding complexes between the enzyme and the substrate; thus, the digestion rate was enhanced. The possible interaction model is discussed in more detail in the Supporting Information.

The results of Y160A, W170A and F172A variants in Figure S8 indicated that the above π–π stacking interactions might significantly influence not only the proportion of the productive and non-productive binding but also the activity of λ exo. According to the crystal data, the three amino acid residues that we have changed (Y160, W170 and F172) were not directly involved in binding to the bases or phosphate backbone in the substrate DNA or in the hydrolysis of the phosphodiester bond. Little information has been reported regarding the influences of these amino acid residues on the activity of λ exo. We infer that the local conformation near the active site of these variants might have changed, leading to low activity on the PM duplexes. By using a higher concentration of the variants, we verified the mismatch-induced acceleration effect on the digestion of dsDNA substrates containing internally labeled groups on the bases (Table 3). In view of the low activity of these variants on the PM substrates, more non-productive binding complex might have been formed between the λ exo variants and the PM substrate. In the presence of the 2-mismatched base pair, the additional interactions between the label and the amino acid residues that contained a conjugated structure might have facilitated the formation of more productive binding complexes between the enzyme and the substrate; thus, the digestion was promoted (Supplementary Scheme S2). For those DNA duplexes containing a label without the conjugated structure, no additional interactions were provided by the chemical label, so the PM and 2-mis duplex substrates showed similar relative rates of digestion by the WT-2 and λ exo variants.

CONCLUSION

Detailed investigations on the interactions between λ exo and diverse dsDNA substrates revealed two unexpected new properties and digestion mechanisms of λ exo. First, the length of the free portion of the 5′-end strand in the DNA duplex plays an essential role in the initiation of the digestion reactions by λ exo. For a 5′ protruding end with a 2-nt overhang, hydrophobic groups such as a C6 spacer can displace the 5′-PO_4 end to initiate the DNA digestion at a rate comparable to that of the blunt and recessed 5′-PO_4 ends. For the duplexes with 5′-OH ends, a 3-nt overhang structure at the 5′ end can initiate the digestion reaction at a markedly high rate. An alternative hydrophobic interaction mechanism between λ exo and dsDNA is proposed and is strongly supported by the comparative study of an inactive variant of λ exo. Second, for a DNA duplex containing an internally labeled base and a single mismatched base pair at the 5′ side, the presence of a conjugated structure (e.g. FAM, ROX or BHQ-1) in the label may significantly accelerate the process of digestion of the labeled strand by λ exo. The possible driving force for this is the π–π stacking interactions between the conjugated structures of the label and the aromatic amino acid residues of λ exo, which may stabilize the productive binding between λ exo and the dsDNA substrate and thus promote the digestion process. The precise interaction models for these new properties merit further detailed study with other methods. These new findings significantly

broaden our knowledge of the interactions between λ exo and nucleic acids, which is important not only for elucidating the complicated *in vivo* DNA repair pathways but also for developing more powerful enzymatic tools for the processing of nucleic acid molecules in various *in vitro* applications.

SUPPLEMENTARY DATA

Supplementary Data are available at NAR Online.

FUNDING

National Natural Science Foundation of China [81571130100, 21575008]; Beijing Municipal Natural Science Foundation [2184103]; Interdisciplinary medicine Seed Fund of Peking University. Funding for open access charge: National Natural Science Foundation of China.
Conflict of interest statement. None declared.

REFERENCES

1. Little,J.W. (1967) An exonuclease induced by bacteriophage lambda. II. Nature of the enzymatic reaction. *J. Biol. Chem.*, **242**, 679–686.
2. Carter,D.M. and Radding,C.M. (1971) The role of exonuclease and beta protein of phage lambda in genetic recombination. II. Substrate specificity and the mode of action of lambda exonuclease. *J. Biol. Chem.*, **246**, 2502–2512.
3. Muniyappa,K. and Radding,C.M. (1986) The homologous recombination system of phage lambda. Pairing activities of beta protein. *J. Biol. Chem.*, **261**, 7472–7478.
4. Poteete,A.R. (2001) What makes the bacteriophage lambda Red system useful for genetic engineering: molecular mechanism and biological function. *FEMS Microbiol. Lett.*, **201**, 9–14.
5. Kovall,R.A. and Matthews,B.W. (1998) Structural, functional, and evolutionary relationships between lambda-exonuclease and the type II restriction endonucleases. *Proc. Natl. Acad. Sci. U.S.A.*, **95**, 7893–7897.
6. Steczkiewicz,K., Muszewska,A., Knizewski,L., Rychlewski,L. and Ginalski,K. (2012) Sequence, structure and functional diversity of PD-(D/E)XK phosphodiesterase superfamily. *Nucleic Acids Res.*, **40**, 7016–7045.
7. Dapprich,J. (1999) Single-molecule DNA digestion by lambda-exonuclease. *Cytometry*, **36**, 163–168.
8. Matsuura,S., Komatsu,J., Hirano,K., Yasuda,H., Takashima,K., Katsura,S. and Mizuno,A. (2001) Real-time observation of a single DNA digestion by lambda exonuclease under a fluorescence microscope field. *Nucleic Acids Res.*, **29**, e79.
9. Subramanian,K., Rutvisuttinunt,W., Scott,W. and Myers,R.S. (2003) The enzymatic basis of processivity in lambda exonuclease. *Nucleic Acids Res.*, **31**, 1585–1596.
10. Pan,X., Smith,C.E., Zhang,J., McCabe,K.A., Fu,J. and Bell,C.E. (2015) A structure-activity analysis for probing the mechanism of processive double-stranded DNA digestion by lambda exonuclease trimers. *Biochemistry-US*, **54**, 6139–6148.
11. van Oijen,A.M., Blainey,P.C., Crampton,D.J., Richardson,C.C., Ellenberger,T. and Xie,X.S. (2003) Single-molecule kinetics of lambda exonuclease reveal base dependence and dynamic disorder. *Science*, **301**, 1235–1238.
12. Perkins,T.T., Dalal,R.V., Mitsis,P.G. and Block,S.M. (2003) Sequence-dependent pausing of single lambda exonuclease molecules. *Science*, **301**, 1914–1918.
13. Conroy,R.S., Koretsky,A.P. and Moreland,J. (2010) Lambda exonuclease digestion of CGG trinucleotide repeats. *Eur. Biophys. J.*, **39**, 337–343.
14. Mattes,W.B. (1990) Lesion selectivity in blockage of lambda exonuclease by DNA damage. *Nucleic Acids Res.*, **18**, 3723–3730.
15. Mitsis,P.G. and Kwagh,J.G. (1999) Characterization of the interaction of lambda exonuclease with the ends of DNA. *Nucleic Acids Res.*, **27**, 3057–3063.
16. Lee,G., Yoo,J., Leslie,B.J. and Ha,T. (2011) Single-molecule analysis reveals three phases of DNA degradation by an exonuclease. *Nat. Chem. Biol.*, **7**, 367–374.
17. Court,D.L., Sawitzke,J.A. and Thomason,L.C. (2002) Genetic engineering using homologous recombination. *Annu. Rev. Genet.*, **36**, 361–388.
18. Sharan,S.K., Thomason,L.C., Kuznetsov,S.G. and Court,D.L. (2009) Recombineering: a homologous recombination-based method of genetic engineering. *Nat. Protoc.*, **4**, 206–223.
19. Rhee,H.S. and Pugh,B.F. (2011) Comprehensive genome-wide protein-DNA interactions detected at single-nucleotide resolution. *Cell*, **147**, 1408–1419.
20. Branton,D., Deamer,D.W., Marziali,A., Bayley,H., Benner,S.A., Butler,T., Di Ventra,M., Garaj,S., Hibbs,A., Huang,X. *et al.* (2008) The potential and challenges of nanopore sequencing. *Nat. Biotechnol.*, **26**, 1146–1153.
21. Song,C. and Zhao,M.P. (2009) Real-time monitoring of the activity and kinetics of T4 polynucleotide kinase by a singly labeled DNA-hairpin smart probe coupled with lambda exonuclease cleavage. *Anal. Chem.*, **81**, 1383–1388.
22. Xiao,X.J., Zhang,C., Su,X., Song,C. and Zhao,M.P. (2012) A universal mismatch-directed signal amplification platform for ultra-selective and sensitive DNA detection under mild isothermal conditions. *Chem. Sci.*, **3**, 2257–2261.
23. Wu,T.B., Xiao,X.J., Zhang,Z. and Zhao,M.P. (2015) Enzyme-mediated single-nucleotide variation detection at room temperature with high discrimination factor. *Chem. Sci.*, **6**, 1206–1211.
24. Wu,T.B., Xiao,X.J., Gu,F.D. and Zhao,M.P. (2015) Sensitive discrimination of stable mismatched base pairs by an abasic site modified fluorescent probe and lambda exonuclease. *Chem. Commun.*, **51**, 17402–17405.
25. Kovall,R. and Matthews,B.W. (1997) Toroidal structure of lambda-exonuclease. *Science*, **277**, 1824–1827.
26. Zhang,J.J., McCabe,K.A. and Bell,C.E. (2011) Crystal structures of lambda exonuclease in complex with DNA suggest an electrostatic ratchet mechanism for processivity. *Proc. Natl. Acad. Sci. U.S.A.*, **108**, 11872–11877.
27. Yoo,J. and Lee,G. (2015) Allosteric ring assembly and chemo-mechanical melting by the interaction between 5′-phosphate and lambda exonuclease. *Nucleic Acids Res.*, **43**, 10861–10869.
28. Marras,S.A., Kramer,F.R. and Tyagi,S. (2002) Efficiencies of fluorescence resonance energy transfer and contact-mediated quenching in oligonucleotide probes. *Nucleic Acids Res.*, **30**, e122.
29. SantaLucia,J. Jr and Hicks,D. (2004) The thermodynamics of DNA structural motifs. *Annu. Rev. Biophys. Biomol. Struct.*, **33**, 415–440.
30. Fersht,A. (1984) *Enzyme Structure and Mechanism*, 2nd edn.. W. H. Freeman.